HOLLOW ATOMS (IONS) ABOVE AND BELOW THE SURFACE

Y.Yamazaki, S.Ninomlya, F.Koike*, H.Masuda**, T.Azuma, K.Komaki,
K.Kuroki***, and M.Sekiguchi+
Institute of Physics, Univ.Tokyo, Komaba, Tokyo 153
* Physics Laboratory, School of Medicine, Kitasato University, Sagamihara, Kanagawa 228
** Dept. Industrial Chemistry, Tokyo Metropolitan University, Hachioji, Tokyo 192-03
*** National Research Institute of Police Science, Chiyoda, Tokyo 100
+ Institute for Nuclear Study, University of Tokyo, Tanashi, Tokyo 188

Abstract

The Interaction of slow highly-charged ions with surfaces is discussed for thin microcapillary foils as well as for flat metal plates. The former provides information on hollow atoms (ions) in the first generation (i.e., above surface). In contrast, the latter is suitable to investigate those in the second generation (i.e., at or below surface). About 1% of 2.1 keV/u N^{6+} ions transmitted through the microcapillary are found to capture at least one electron, which is consistent with the prediction of the classical over-barrier model. The charge state distribution is found to be a very weak function of the exiting charge, which is quite different from that transmitted through a thin foil or that specularly reflected from a surface. N and Ne K X-rays emitted from the downstream of the target show that ~1% of the charge changed ions are in extremely stabilized states with lifetimes of ~ns keeping an innershell orbital open. Further, the relaxation dynamics of hollow atoms in the second generation are studied through measurements of L-X-rays from Ar ions as a function of L-shell hole numbers.

Introduction

The formation and decay dynamics of hollow atoms produced by the interaction of slow highly-charged ions (HCIs) with surfaces have been studied considerably in recent years through measurements of charge state and angular distributions of the ions, X-rays and Auger electrons, sputtering, etc. [1-10]. When a slow multiply charged ion approaches a solid surface, target valence electrons are preferentially transferred into excited states of the ion [11]. Such an atom (ion) with multiply-excited electrons and innershell vacancies is the "hollow atom (ion)" referred to above, which is expected to be a new type of atomic state.

An effective potential Φ (x, y, z) for an electron at (x, y, z) from the surface of a metal with an ion at Z_p is given by,

$$\Phi(x,y,z) = \frac{-q}{\left(x^2+y^2+\left(z-Z_p\right)^2\right)^{1/2}} + \frac{q}{\left(x^2+y^2+\left(z+Z_p\right)\right)^{1/2}} - \frac{1}{4z}, \qquad (1)$$

where q is the charge state of ions. A schematic drawing of Φ (x, y, z) is given in fig.1, which indicates an appearance of a saddle point. As Z_p gets smaller the saddle point gets deeper. The classical over-barrier model [11] predicts that resonant charge transfer starts when the saddle point depth becomes comparable to the work function of the target, i.e., the critical distance d_r for the resonant charge transfer is given by ~ $(2q)^{1/2}/W$, where W is the binding energy of the target valence electrons (physical quantities are given in atomic units unless otherwise noted.). In this case, the principal quantum number is estimated to be $n_r \sim q/\{2W(1+(q/8)^{1/2})\}^{1/2}$. As is imagined, the radii of the resultant excited states are comparable to d_r . Due to the interaction of the ion with its image charge, the ion gains kinetic energy of ~ $2^{-5/2}q^{3/2}$ W. When the ion further

approaches the surface, the barrier lowers and the energy level of the ion shifts upward due to the image charge, resulting in resonant charge transfers to states with $n < n_r$, which causes release of some electrons already in highly excited states. Such a successive lowering of the states in which target valence electrons are transferred is expected to last until the ion reaches the surface as far as the target electron states are in resonance with the state of the ion in question, i.e., the above scenario is valid for high q, where the density of electronic states is high enough to guarantee classical treatments of the process. In this case, the key parameter to control the phenomena is the charge state q, which is compared with the neutralization of singly charged ions where the binding energies of the ions play an important role [12].

Recently, Burgdoerfer et al. [13], Arnau et al. [14], and Arnau [15] showed prescriptions to handle energy levels of HCIs at or below the surface. Qualitatively, target valence electrons could dynamically screen the ion charge with the screening length of $\lambda_{sc} \sim \upsilon_F/\omega_{pl} \sim r_s^{1/2}$, where υ_F, ω_{pl} and r_s are the fermi velocity, plasmon frequency and electron radius of the target, respectively. If the incident ion has a bound state at or below the surface, its orbital radius should be smaller than or at the most comparable to λ_{sc}. The largest possible principal quantum number of the bound electron n_1 could be crudely estimated assuming the atomic radius $n_1^2/q(n_1)$ to be $\sim \lambda_{sc}$, where $q(n_1)$ is an effective charge of the ion in the solid for the bound electron in question. In this case, $q(n_1)$ is of the order of 1, i.e., the energy level of the state with $n \lesssim n_1$ at or below the surface is considerably promoted as compared with that in vacuum. In this way, some deep bound states with $n_2 \lesssim n \lesssim n_1$ are resonantly filled. When the incident ion has holes at states with principal quantum numbers lower than n_2, hollow atoms are temporalily formed even below the surface, which relax to their ground states emitting Auger electrons and/or X-rays [1,7]. Such a hollow atom formed at or below the surface is referred to as a hollow atom in the second generation (HA2), hereafter. On the other hand, that formed above the surface is referred to as a hollow atom in the first generation (HA1), hereafter. For example, in the case of Ne^{9+} on a metal surface, d_r is ~ 10 Å, $n_r \sim 10$, the energy gain due to the image acceleration is ~ 30eV, and $n_2 \sim 2$. The time interval between the hollow atom formation and its arrival at the surface τ_1 is at the longest 10^{-14}- 10^{-13}s, which is possibly shorter than its lifetime, i.e., it is difficult to study the intrinsic nature of the hollow atom when flat surface targets are used.

The major purpose of the present report is to propose a new technique to avoid the above difficulties and to demonstrate its uniqueness to prepare excited states related to HA1 and to extract them in vacuum. As is seen from the above scenario, HA1 had better be called "dynamic hollow molecules". In this respect, the present report discusses, for the first time, isolated hollow atoms in vacuum.

Microcapillary Target

1. Hollow atoms in the first generation

The validity of the classical over-barrier model to predict d_r had been clearly demonstrated through measurements, e.g., of the angular shift of specularly reflected ions under glancing incidence [4], and of velocity dependent secondary electron yields [6]. On the other hand, information on the character of HA1 has been very limited, which was obtained through measurements of projectile Auger electrons [2] or X-rays [16] under glancing scattering configuration or under slow ion impact [5]. In this case, the time for the ion to be HA1 is somewhat extended, and more signals from HA1 are expected. However, as is discussed in the introduction, the image acceleration limits the available time to observe HA1, which is in the end turned into HA2 at or below the surface. (fig.2(a)) Summarizing, there are two major difficulties

in studying HAI with flat surface targets, i.e., signals from HA2 are typically stronger than those from HA1, and the survival times of HA1 are possibly too short for their intrinsic nature to be studied.

In order to avoid the above difficulties and to preferentially prepare HA1 suppressing production of HA2, thin foils with straight multi-microcapillaries [17,18] are employed as targets [19]. (fig.2(b)) When HCIs impinge on the target in parallel with the capillary axis, a part of HA1 formed in the capillary could pass through it before hitting the capillary wall. In this case, HA1 is extracted in vacuum, the character of which could fully be studied employing established reliable techniques. In the present report, a thin (~10 μ m) Al_2O_3 foil with its capillary diameter of ~100nm and a thin (~1.5 μ m) Ni foil with the diameter of ~250nm are used as targets. Figure 3 shows SEM (scanning electron microscope) images of (a) the Ni and (b) the Al_2O_3 foils. The geometrical openings of the Al_2O_3 and Ni foils are ~20% and ~50%, respectively, which are compared with the experimental ion transmission fractions of ~1% and ~15%, respectively. It is noted that the transmission of ions through the Al_2O_3 target was observed only when charging up of the target is avoided by an electron shower. For 2,1keV/u N^{6+} ions on the Ni target, the charge changed fraction of the total transmitted ions is found to be ~1%. As ions passing near the capillary wall at a distance shorter than d_r are expected to capture electrons resonantly into their excited states, the charge changed fraction is estimated to be ~$2d_r/r$~1,3%, which is in good accord with the observation.

2. Experimental Setup

Slow highly charged ions supplied from a HyperECR of the Institute for Nuclear Study, University of Tokyo [20], are charge-state selected by an analyzing magnet, collimated by a four jaw slit system, and introduced into a target chamber which is evacuated down to ~10^{-9} Torr. Considering that the outgassing from the capillary wall is known to be ~10^{-8} Torr ℓ/cm^2·sec or less [21] and the conductance of the capillary is ~$10^{-11}\ell$/sec, the pressure in the capillary is estimated to be ~10^{-5} Torr, i.e., electron capture events from the residual gas in the capillary are negligibly small. The capillary target is installed on a manipulator with 3 dimensional linear motions and 2 dimensional angular motions ("rotation" and "tilt" in flg.4). As shown in fig.4, a Si(Li) X-ray detector is installed near the target. The shield A located between the target and the X-ray detector is movable along the beam axis and is used to limit the detection region for delayed X-ray measurements. The position z of the shield A is referred to with respect to the target. At z=0, no X-rays emitted upstream of the target are observed.

3. Charge state distribution

The charge state distribution f(q) for 2,1keV/u N^{6+} ions transmitted through the Ni capillary is shown in fig.5. It is seen that f(q) varies fairly slowly from q=0 to q=5. One may compare this distribution with that of ions transmitted through a foil or with that of ions specularly reflected from a surface for glancing incidence. As an example, the charge state distribution for 15keV/u N ions transmitted through a thin carbon foil [22] is plotted in fig.5 with a thick solid line. Although the ion velocity is much higher than that in the present conditions, the distribution shows a peak at q=1 and only charge states with q=0-2 are predominantly populated. In the case of glancing scattering of 3,75keV/u O^{8+} on Au(110), where the scattering configuration is very similar to the present capillary transmission except that all the ions eventually hit the surface, only a few % of the reflected particles are found to be positively charged [23]. It is worthy to be noted that the charge state distribution of Ar ions passed through

gaseous C_{60} [24] shows qualitative similarities observed for the capillary targets. These observations strongly support the idea that the capillary foil is an effective and unique target for supplying some limited number of electrons keeping the charge state distribution away from the equilibrium.

4. X-ray Spectra

To penetrate further into the interaction of slow HCIs with microcapillaries, K-shell filling processes were studied through measurements of X-rays emitted from transmitted ions in flight. Figure 6(a) shows an energy spectrum of Ne K X-rays emitted downstream of the Ni microcapillary target for 9keV/u Ne^{9+} ions. The peak around 900eV corresponds to KL transitions of Ne and the broad bump around 1100eV corresponds to KM and higher transitions. If the ion beam is blocked by tilting or rotating the target, no X-rays are observed, confirming that atoms (ions) with K-shell vacancy on flight emit X-rays downstream of the target. As it takes $\sim 10^{-12}$ sec for the ions to pass through the capillary, excited states which have shorter lifetimes than this do not considerably contribute to the spectrum.

Figure 6(c) shows a spectrum of X-rays observed when the ion hits a flat Al plate, i.e., X-rays are primarily emitted from HA2. In this case, the peak energy is seen to be ~50eV lower than the above. Comparison of the KL transition energies with theoretical values [25] shows that an average number of L shell electrons n_L at the moment of X-ray emission for the capillary transmission case is much less than that for the flat target case. A qualitatively similar behaviour was reported by Schulz et al. for Ar K X-rays [26]. Assuming an isotropic angular distribution, the total KL X-ray yield per incident ion for the flat target is roughly estimated to be $\sim 10^{-3}$, which is an order of magnitude smaller than the fluorescence yield of Ne^0 with a K hole. It is noted that such a reduction of the fluorescence yield was also inferred for M X-rays of U [27]. The energy resolution of the Si(Li) detector is not high enough to specify the number of electrons in M- and higher shells during KL transitions, i.e., the charge state at the moment of X-ray emission is not known from the present measurements. Actually, Auger electron spectroscopy is much more sensitive to the number of outer electrons because the Auger electron energy is considerably influenced by outer screening.

In the case of the capillary transmitted ions, the K-X-ray yield per charge changed ion is found to be ~1%, which is more than an order of magnitude higher than those for the flat Al target. Considering that even the lifetime of 2p Ne^{9+} is $\sim 10^{-13}$ sec, where only radiative transitions are allowed, and the observed X-rays are emitted more than 10^{-12} sec after the production of the corresponding excited states, the yield of ~1% is considered to be unusually high. Again, this finding is a clear indication that very mild collisions are preferentially realized with the microcapillary targets.

5. Lifetimes of the K-shell hole of capillary transmitted N and Ne

The lifetimes of the excited states with a K-hole are determined by measuring the intensity of X-rays emitted from ions at a distance x or more from the capillary target, which is referred as an integrated delayed X-ray yield,

$$\eta(t_d) = \eta(x / \upsilon) = \int_{x/\upsilon}^{\infty} \zeta(x' / \upsilon) dx' / \upsilon \ , \qquad (2)$$

where $\zeta(x' / \upsilon)$ is the differential X-ray yield at x' from the target along the ion path, and υ the projectile velocity [18]. If the excited states consist of several components which decay

exponentially, $\zeta(t)$ and $\eta(t)$ are expressed,

$$\zeta(t) = \sum A_k / a_k \exp(-t / a_k) ,$$
$$\eta(t) = \sum A_k \exp(-t / a_k) ,$$

where A_k is the population fraction of the k-th component, and a_k its lifetime. It is seen that the relative population of each component is directly known from $\eta(t)$.

Figure 7 shows the delayed X-ray yield $\eta(t_d)$ for incident ions of 9keV/u N^{6+}, and 9keV/u and 2,7keV/u Ne^{9+}. The time resolution of this measurement for 9keV/u ion was ~0,3ns. The delayed yields of 2,7keV/u and 9keV/u Ne^{9+} are almost the same with each other within the experimental accuracy, showing two exponentially decreasing components with lifetimes of ~0.5ns and ~2.5ns. Previous measurements performed, having better time resolution (~0,1ns), with the Al_2O_3 target show that the 0,5ns component is further decomposed into at least two components with lifetimes of <0,1ns and ~0,8ns [19]. From fig.7 and fig.4 of ref.19, the relative fractions of the <0,1ns, 0,8ns, and 2,5ns components are estimated to be ~5:1:1. The spectrum of X-rays emitted from the 2,5ns component (9keV/u Ne^{9+} transmitted through the Ni target for t_d =2,3ns) is shown in fig.6(b). Comparison between figs.6(a) and 6(b) indicates that the spectrum shape of KL X-rays does not depend very much on the components. In other words, the number of L-shell electrons of the 2,5ns component is similar to that of the 0,1ns and 0,8ns components. It is seen that the KM and higher X-rays diminish much quicker than the KL X-rays. In the case of 9keV/u N^{6+} transmitted through the Ni target, at least two components with lifetimes of ~0,8ns and ~4ns are discernible with a relative fraction of ~2:1.

Theoretical evaluation of the lifetimes and transition energies [19] for two to four electron systems of Ne suggests that Ne^{7+} 1s2s2p ^4P states are the potential candidates for the observed 0,8ns component. The total (radiative and Auger) lifetimes are predicted to be 0,4 (1,6 and 0,43), 0.6 (0,71 and 3,8) and 12 (0 and 12) ns for Ne^{7+} 1s2s2p $^4P_{1/2}$, $^4P_{3/2}$, and $^4P_{5/2}$ states, respectively. The decay of $^4P_{5/2}$ state is possible only through Auger electron emission. The dominant radiative decay channels of $^4P_{1/2}$ and $^4P_{3/2}$ states are to $1s^22s\ ^2S_{1/2}$ with X-ray energy of 895,0 eV. Theoretical evaluation of lifetimes suggests that considerable stabilization of multiply excited atoms (ions) is realized for states with the highest spin multiplicities. All the electron spins are aligned, and all the shells are less than half-filled, which actually explains why the energy of KL X-rays observed downstream of the capillary target always indicates a low number of L-shell electrons at the moment of the transition. For the transitions to take place from these spin aligned excited states, mixing of spin-flipped components in the initial and/or the final states of the active electron is essential, which is induced by the l·s interaction. Because the l·s interaction becomes less important for higher excited states, the observed dominance of the KL transition over the KM and higher transitions at t_d >1ns (fig.6(b)) seems plausible. The 2,5ns component is difficult to explain in terms of the core electron configurations surveyed here, implying that some cascading process from higher lying states with longer lifetimes plays a role, i.e., several extra electrons could be held in high Rydberg orbitals to form more neutralized Ne ions. Actually, recent coincidence measurements show that K X-rays from N and Ne ions transmitted through the Ni target are not only emitted from 2 or 3 electron systems but also from 5 or more electron systems [28].

3. Flat Surface Experiment - - - Hollow atoms In the second generation

Hollow atoms in the second generation have been studied, e.g., through measurements of incident angle dependences of Auger electron yields [7] and X-ray yields [1], etc.

Here we discuss the behaviour of L-X-rays instead of K X-rays, because the number of

available L- holes is much larger than that of K- holes, which allows us to approach the problem from a different point of view [29]. To discuss the fate of HCIs at or below the surface (i.e., in the second generation), energy spectra of L-X-rays emitted from Ar^{q+} ions (q=9-14), $dY(n_L)/dE$, are measured, where n_L is the number of the L-shell holes of the incident ion (n_L=q-8=1-6), and shown in fig.8(a). Figure 9 shows the total yields of Ar L X-rays integrated from 150eV to 800eV as a function of the kinetic energy of Ar ions. The yields for q=7 and q=8 increase monotonically with the kinetic energy. On the other hand, only very weak dependences are observed for $q \geqq 11$. An Ar^{q+} with $q \geqq 9$ has L-shell hole from the beginning. Therefore, when an HA1 or HA2 is formed, L X-ray emission is possible without excitation.

As Ar L-shell holes are too deep to be resonantly filled even with the promotion discussed in the introduction, they are filled via Auger electron or X-ray emissions one by one, i.e., typically n_L steps are involved to fully fill the L-shell holes. On the other hand, M- or higher shells could be filled (quasi-)resonantly, i.e., the relaxation time of the outershell electrons is expected to be shorter than the L-shell filling process. Therefore, the outershell electron configuration is more or less in equilibrium at the moment of each L-shell filling process, and the difference spectra defined by $dI(n_L)/dE \equiv dY(n_L)/dE - dY(n_L - 1)/dE$ are expected to represent X-rays emitted when the number of L-shell holes changes from n_L to n_L-1 independent of the incident charge state of the ion. Figure 8(b) shows $dI(n_L)/dE$ for 3keV/u Ar^{q+} bombarding a Be target [29], the peak energy of which becomes higher as n_L increases. Comparison with a theoretical evaluation shows that the observed X-rays belong primarily to 3s-2p transitions of $Ar^{(nL+7)+}$ for all n_L. The influence of the number of outershell electrons are again too small to be detected. The contribution of X-rays due to 3d-2p transitions is found to be very small for all n_L, which is consistent with a naive expectation that electrons are transferred towards the ion via the potential minimum, which is located on the vertical line from the ion to the surface, that is, the total angular momentum of the transferred electrons with respect to the ion is very small if not zero. The X-ray yield $I(n_L)$ from each L-shell filling process (i.e., the fluorescence yield) is found to be $\sim(1\text{-}4)\times10^{-4}$/Ion, which is more or less consistent with tabulated values, and confirms the assumption that the relaxation times of the outer shell electrons are much faster than the L-shell filling process.

High energy tails seen in fig.8(b) are accounted for by the contribution of 4s-2p and higher transitions. Assuming that only ns-2p transitions are appreciable, the X-ray spectra are decomposed into transitions with different n, employing a Gaussian fitting procedure. The ratios of the yield due to 3s-2p and 4s-2p transitions to the total X-ray yield, are about 80% and 15%, respectively, for all charge states studied.

4. Summary

A technique of using microcapillary foils as targets is shown to provide a new way to effectively produce multiply-excited stabilized atoms (ions), which may be referred to as Beam Capillary Spectroscopy. This combination allows the study of HA1 (hollow atoms (ions) in the first generation) and their relatives in vacuum. Considerable fractions of N and Ne ions transmitted through the microcapillary targets are found to be stabilized keeping a K-shell hole. It is suggested that the formation of high spin multiplicity states with less than half-filled shells are responsible for the stabilization. To study HA2 (hollow atoms in the second generation), Ar^{q+} with various number of L-shell holes are employed. It is shown that there exists qualitative difference in the hole filling processes between the L-shell and the M- and higher shells of Ar.

Acknowledgements

The research is supported by the Grant-in-Aid for Scientific Research on Priority Area, Atomic Physics of Multiply Charged Ions (05238103), and the Grand-in-Aid for Developmental Scientific Research (07555006) from the Ministry of Education, Science, and Culture.

REFERENCES

1. Briand J.P., de Billy L., Charles P. and Essabaa S., Phys.Rev.Lett.:159, 65(1990).

2. Meyer F.W., Overbury S.H., Havener C.C., Zeijlmans van Emmichoven P.A. and Zehner D.M., Phys.Rev.Lett.:723, 67(1991).

3. Andrae H.J. et al., Z.Physlk D:S135, 21(1991).

4. Winter H., Europhys.Lett.:207, 18(1992).

5. Das J. and Morgenstern R., Phys.Rev.A:R755, 47(1993).

6. Aumayr F., Kurz H., Schneider D., Briere M.A., McDonaldJ W., Cunningharn C.E. and Winter H.P., Phys.Rev.Lett.:1943, 71(I993).

7.Koehrbrueck R., Grether M., Spieler A. and Stolterfoht N.,Phys.Rev.A:1429, 60(1994).

8. Folkerts L., Schippers S., Zehner D.M. and Meyer F.W., Phys.Rev.Lett.:204, 74(1995).

9. Kakutani K., Azuma T., Yamazaki Y., Komaki K. and Kuroki K., Jpn.J.Appl. Phys.: L580, 34(1995).

10. Neidhart T., Pichler F., Aumayr F., Winter H.P., Schmid M. and Varga P., Phys.Rev. Lett.: 5280, 74(1995).

11. Burgdoerfer J., Lerner P. and Meyer F.W., Phys. Rev. A:5674, 44(1991).

12. Winter H. Comm.At.Mol.Phys.26(1991) 287.

13. Burgdoerfer J., Reinhold C. and Meyer F.W., Nucl. Instrum. Methods B:415, 98(1995).

14. Arnau A., Zeijlmans van Emmichoven P.A., Juaristi J.I. and Zaremba E., Nucl.Instrum. Methods B: 79, 100(1995).

15. Arnau A., Phys.Rev.A:R3399, 51(1995).

16. d'Etat B., Briand J.P., Ban G., de Billy L., Desclaux J.P. and Brand P., Phys.Rev. A:1098, 48(1993).

17. Masuda H. and Fukuda K., Science: 1466, 268(1995).

18. Masuda H. and Satoh M., Jpn.J.Appl.Phys.: L126, 35(1996).

19. Yamazaki Y., Ninomiya S., Koike F., Masuda H., Azuma T., Komaki K., Kuroki K. and Sekiguchi M., J.Phys.Soc.Jpn.:1199, 65(1996).

20. Sekiguchi M.et al., Proc. 125th Int. Corf. Cyclotrons and Their Applications (World Scientific, Vancouver, 1992) p.326.

21. Yoshimura N.et al., Vacuum (Shinku) 13(1970) 23 (in Japanese).

22. Wlckholm D. and BickelW.S., J.Opt.Soc. Am.:502, 66(1976).

23. Meyer F.W., Folkerts L., Folkerts H.0. and Schippers S., Nucl.Instrum.Methods B:441, 98(1995).

24. Walch B., Cocke C.L., Voelpel R. and Salzborn E., Phys.Rev.Lett.72(1994)1439.

25. Bhalla C.P., Phys.Rev.A:122, 12(1975).

26. Schulz M., Cocke L.C., Hagman S. and Stoeckli M., Phys.Rev.A:1653, 44(1991).

27. Schuch R., Schneider D., Knapp D.A., DeWitt D., McDonald J., Chen M.H., Clark M.W. and Marrs R.E., Phys.Rev.Lett.:1073, 70(1993).

28. Ninomiya S. et al., in preparation.

29. Ninomiya S., Yanlazaki Y. Sawatari K, Irako M., Komaki K., Azuma T., Kurokl K. ■d Sekiguchi M., Nucl.Instrum.Methods B:17, 115(1996).

FIGURE CAPTIONS

fig.1: Schematic drawing of an effective potential $\Phi(x,y,z)$ for an electron at z from a metallic surface with an ion at Z_p.

fig.2: Schematic diagrams drawing the fate of highly charged ions (a) near a flat metallic surface and (b) in a microcapillary target.

fig.3: SEM images [17,18] of (a) Ni and (b) $Al_2 O_3$ capillary targets.

fig.4:A schematic drawing of the experimental setup for the capillary target.

fig.5: An observed charge state distribution f(q) of 2,1keV/u N^{6+} ions transmitted through the Ni capillary target (solid circles). The angular divergence is seen to be bigger for lower exiting charge state, i.e., the real f(q) for q=l-2 could be slightly bigger than those shown here. The thick solid line draws the equilibrium charge state distribution of 15keV/u N ions transmitted through a carbon foil [22]. The thin solid line is to guide the eyes only.

fig.6:(a)The energy spectrum of X-rays emitted from 9keV/u Ne downstream of the Ni microcapillary target at t_d=0. (b)The same as (a) except that t_d=2,3ns. (c)The energy spectrum of Ne X-rays emitted for an A1 plate target. The error bars are statistical. The bars with numbers in the upper part of the figure show predicted energies of KL X-rays [25] with corresponding number of electrons in the L-shell. The arrows indicate the X-ray energies of np- 1s transitions of Ar.

fig.7: Integrated K X-ray yield $\eta(t_d)$ as a function of the distance from the target for 9keV/u N^{6+} (Δ), 9keV/u Ne^{9+} (O), and 2,7keV/u Ne^{9+} (□) transmitted through the Ni multicapillary target [19]. (For details, see the text.)

fig.8: (a) $dY(n_L)/dE$ and (b)$dI(n_L)/dE$ for 3keV/u Ar ions bombarding a flat Be target. The number of incident L-shell holes of each spectrum is n_L =l, 2.5, 4, 5, and 6 from the left to the right in the figure. The bars with numbers in (b) show the transition energies for Ar L X-rays which have core electron configuration in the ground state of $Ar^{(nL+7)+}$ and an electron in the M shell. The spectrum for n_L =2,5 is calculated by {dY(11)/dE- dY(9)/dE}/2 [29].

Fig.9:Ar L X-ray yields for Arq+ on A1 target as a function of the ion kinetic energy:q=7(O), 8(□), 9(Δ), 11(∇), 12($\Diamond$), and 13(©). The yields are measured with the Al window in front of the Si(Li) detector [29].

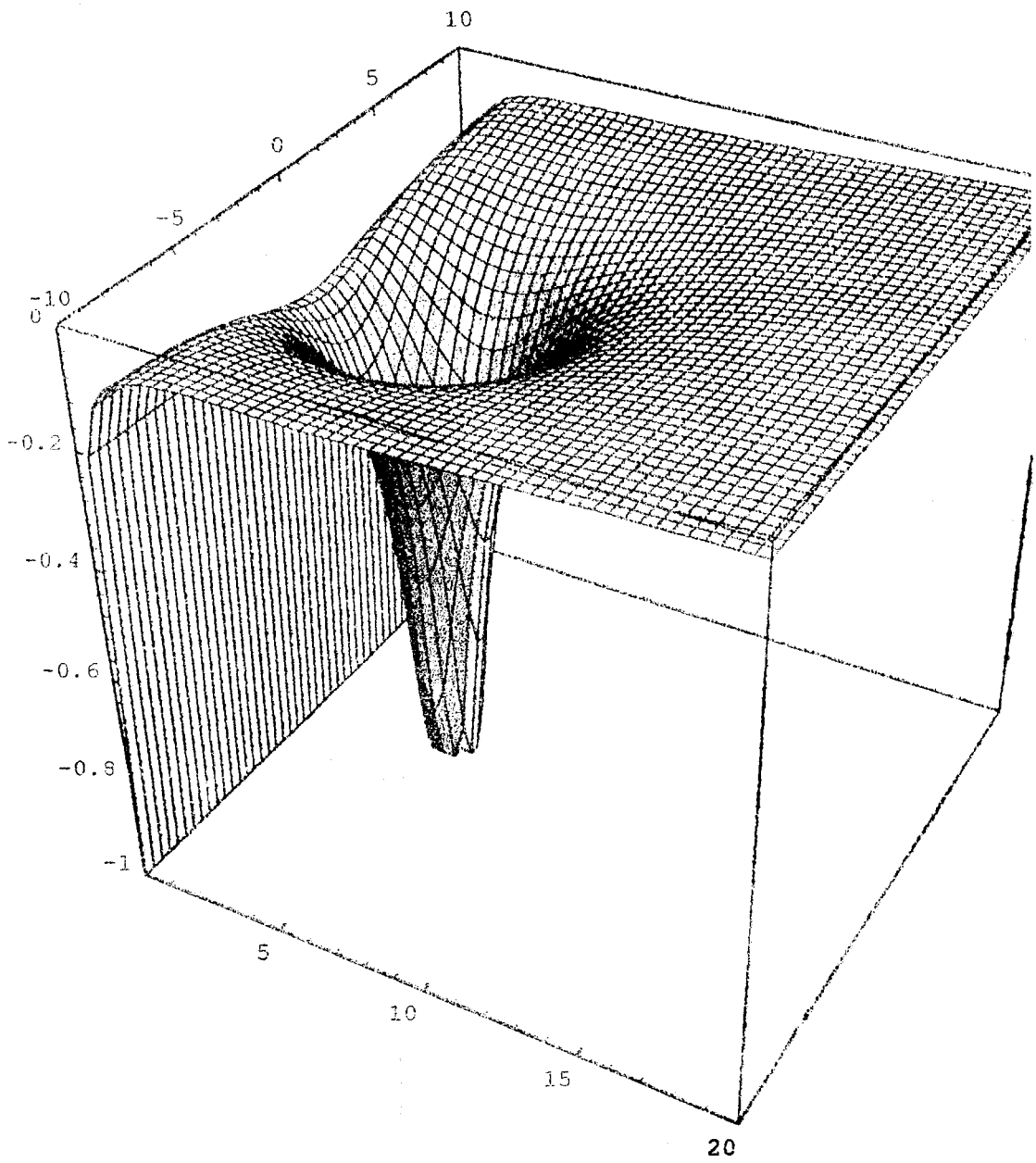

Fig.l.

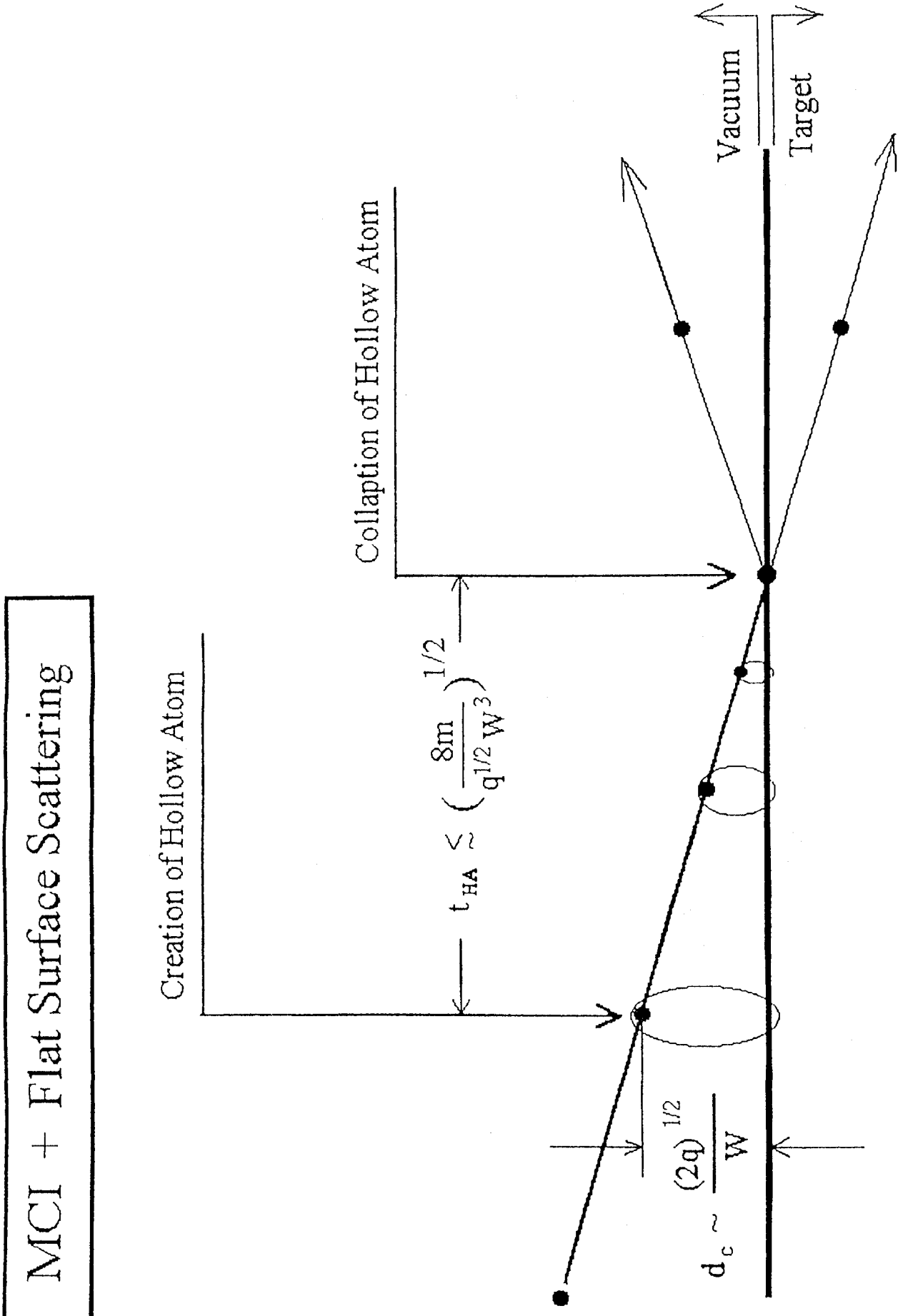
MCI + Flat Surface Scattering
Creation of Hollow Atom
Collaption of Hollow Atom
$t_{HA} \lesssim \left(\frac{8m}{q^{1/2}W^3}\right)^{1/2}$
$d_c \sim \frac{(2q)^{1/2}}{W}$
Vacuum
Target

Fig.2(a).

MCI + Microcapillary Scattering

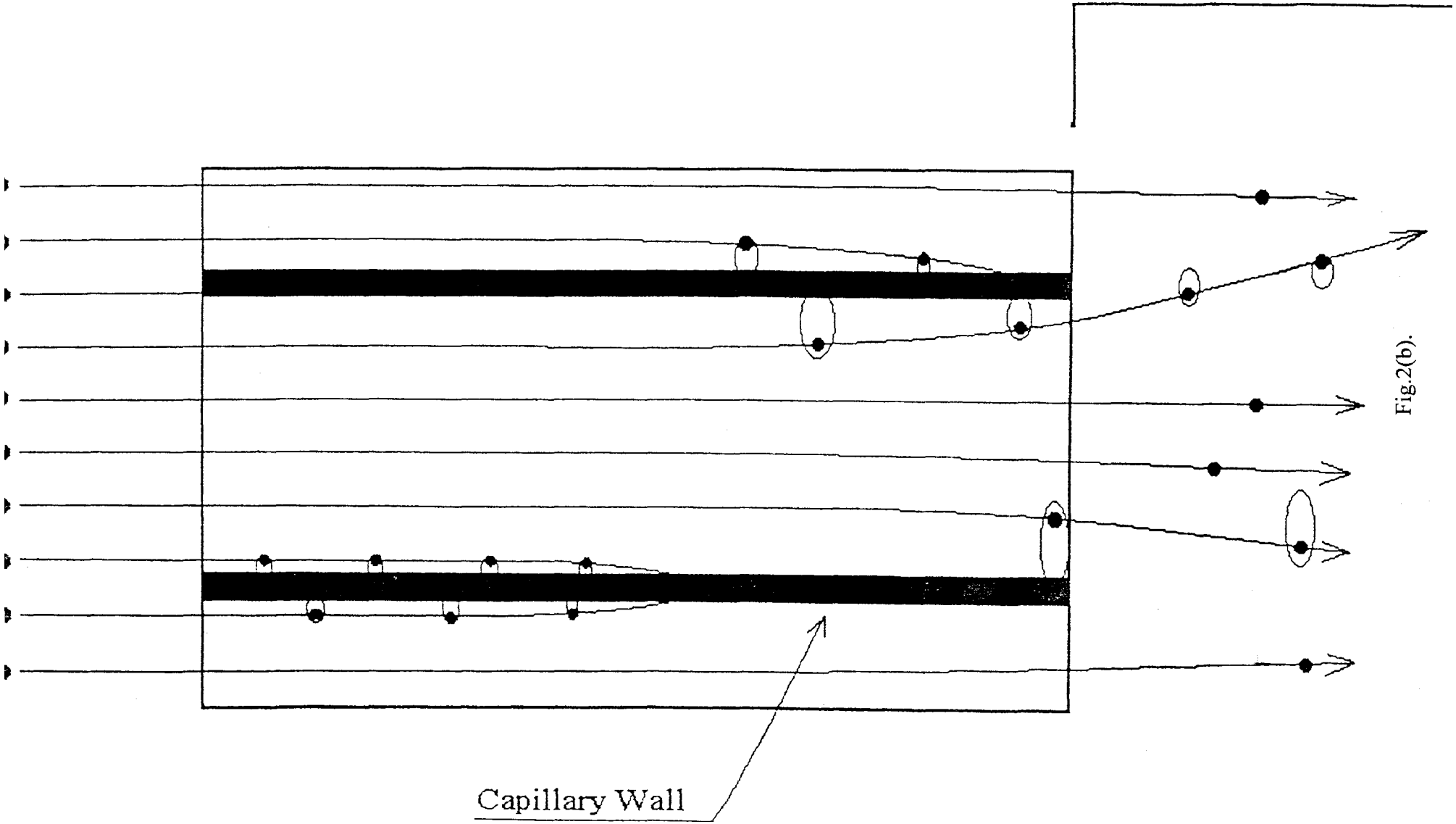

Fig.2(b).

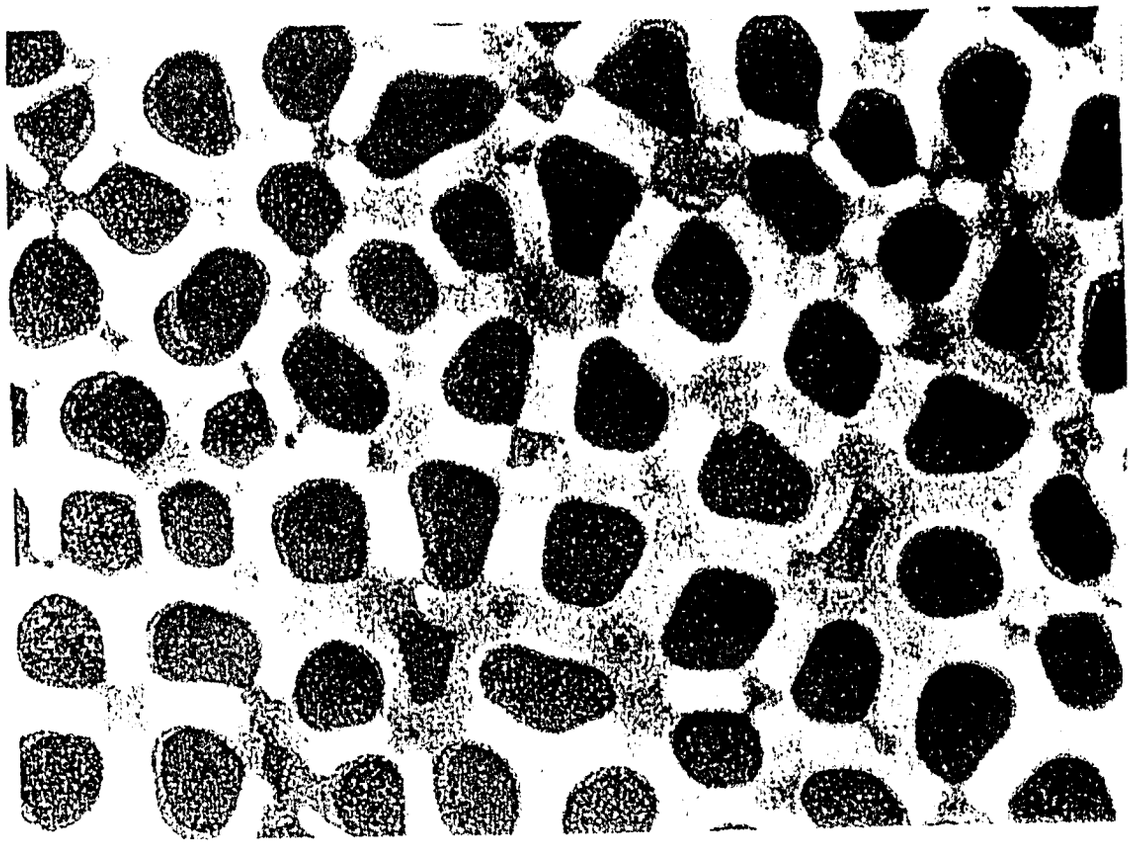

a

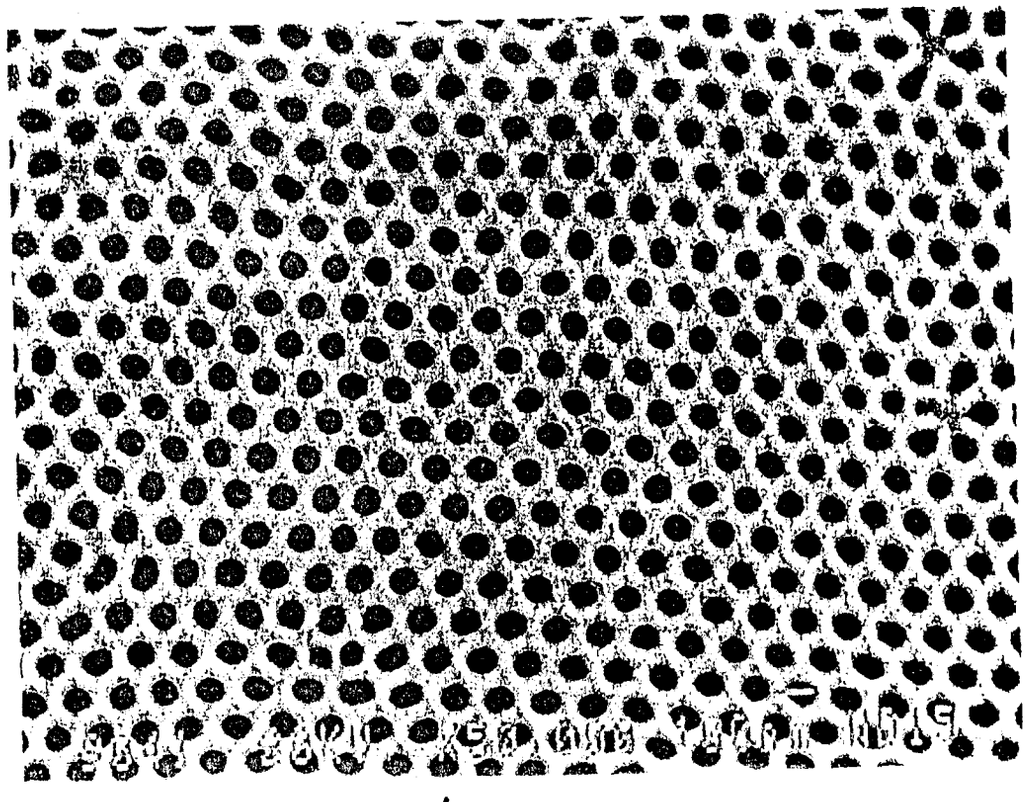

b

1 μm

Fig.3.

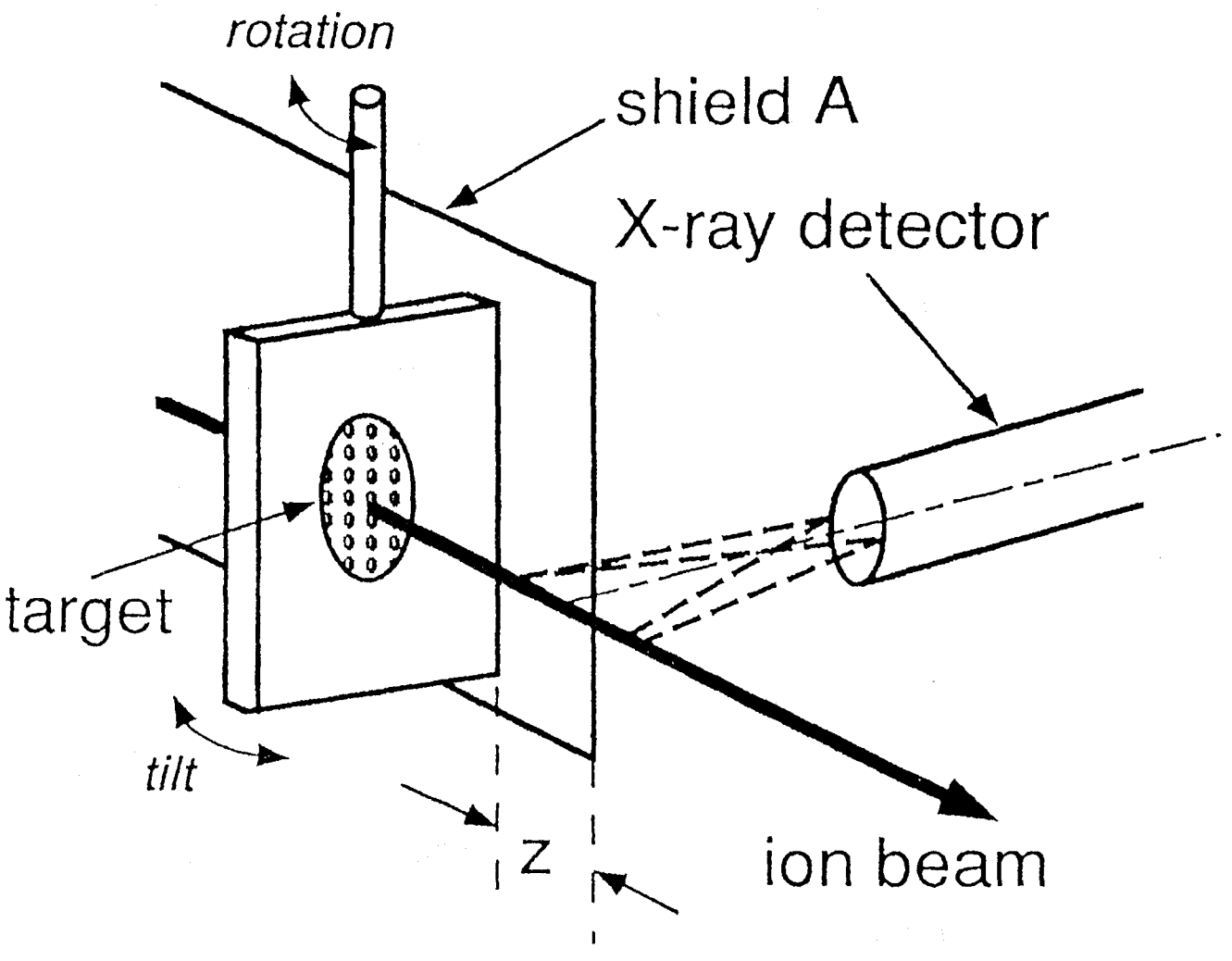

Fig.4.

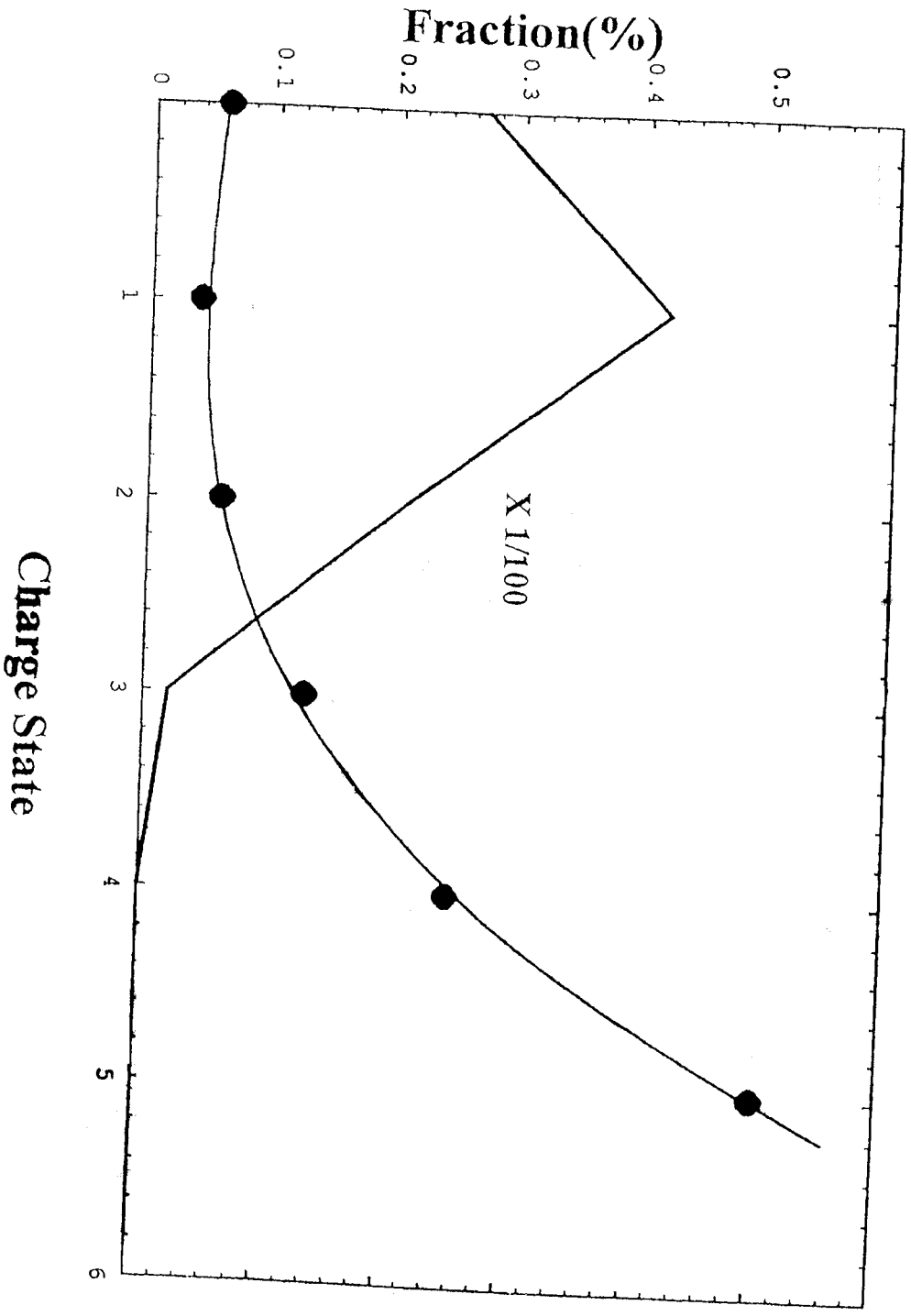

Fig.5.

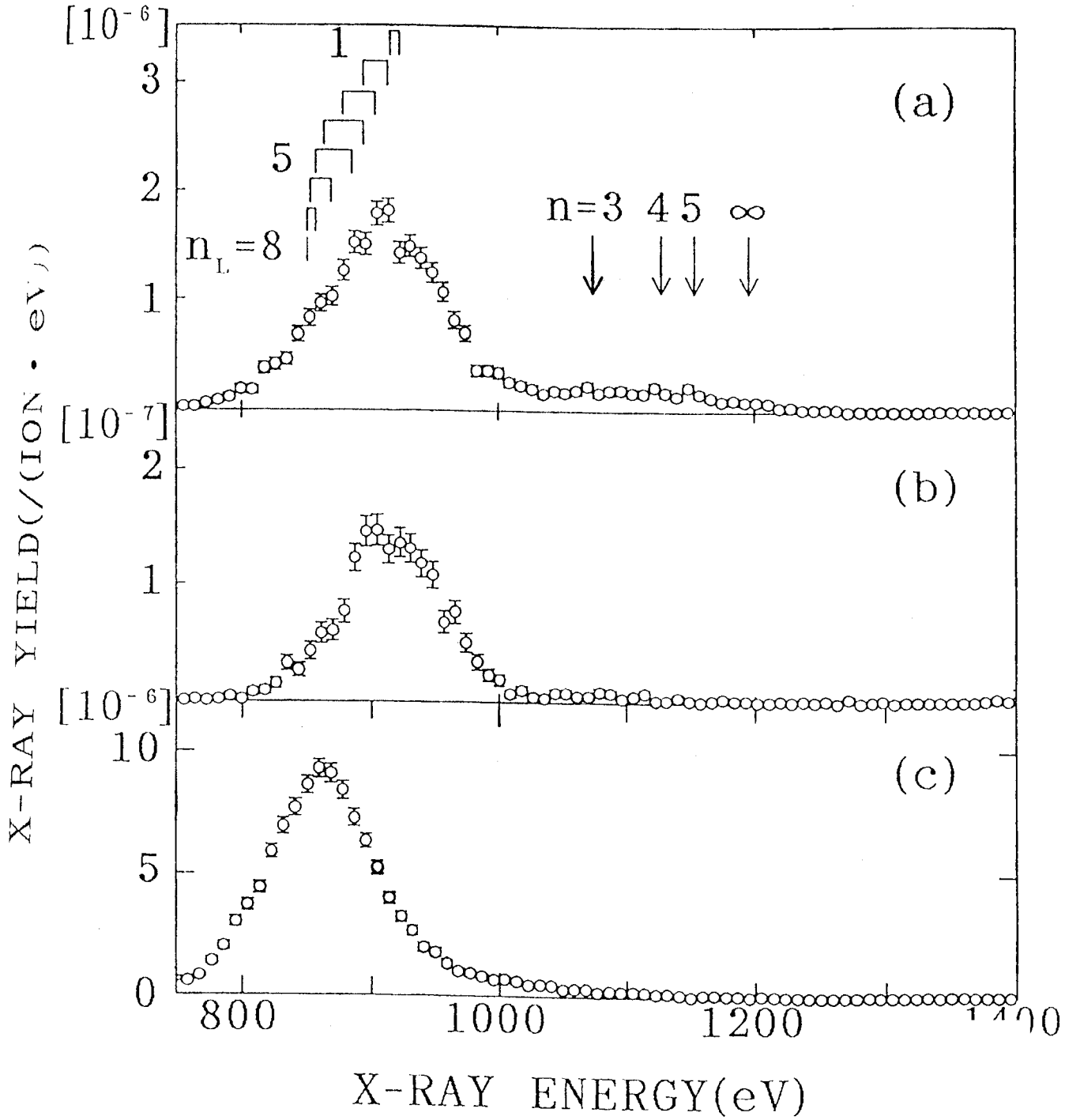
[10⁻⁶]
3
2
1
[10⁻⁷]
2
1
[10⁻⁶]
10
5
0
(a)
(b)
(c)
1
5
n_L=8
n=3 4 5 ∞
X-RAY YIELD(/(ION・eV))
800
1000
1200
X-RAY ENERGY(eV)

Fig.6

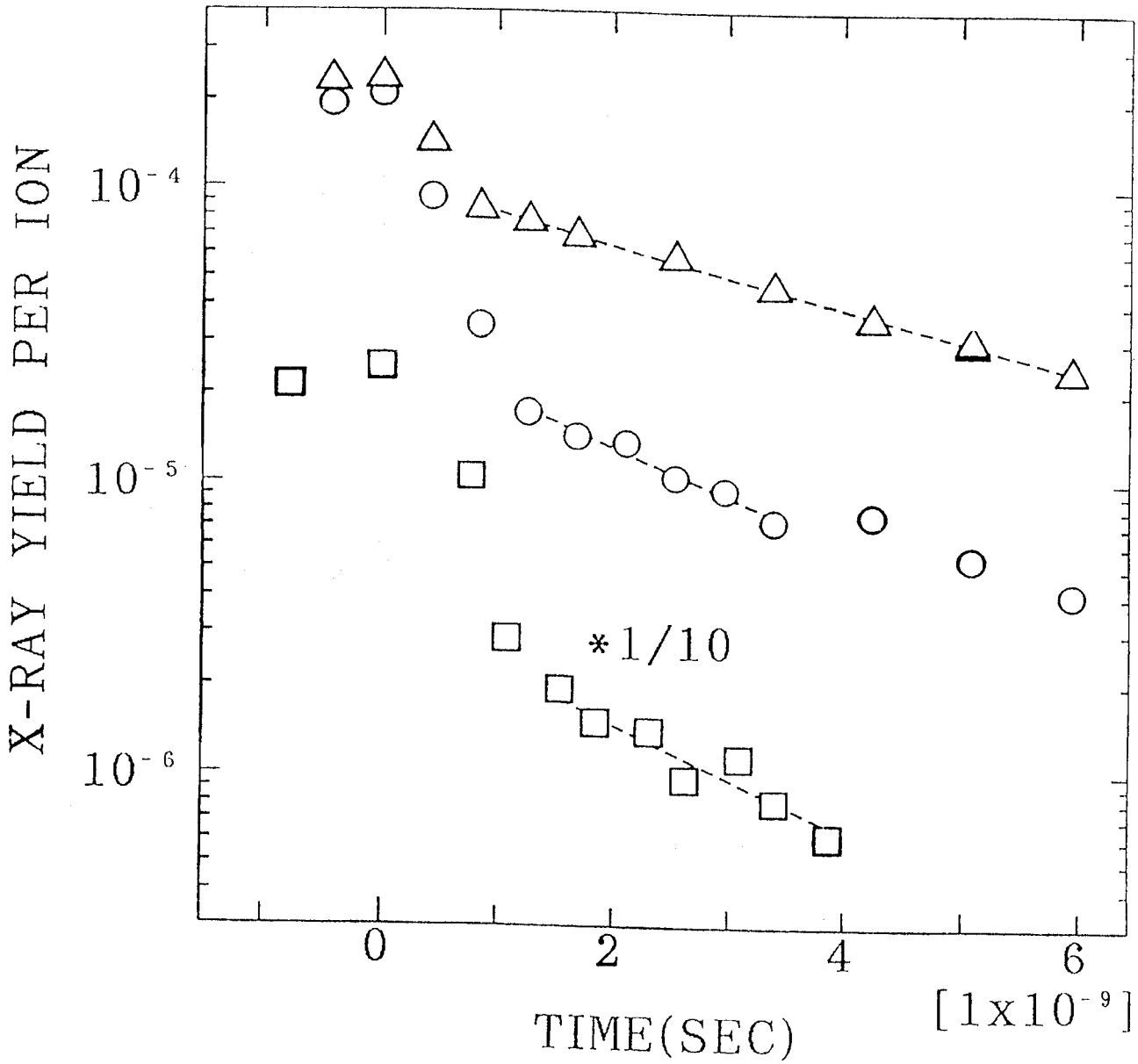

Fig.7.

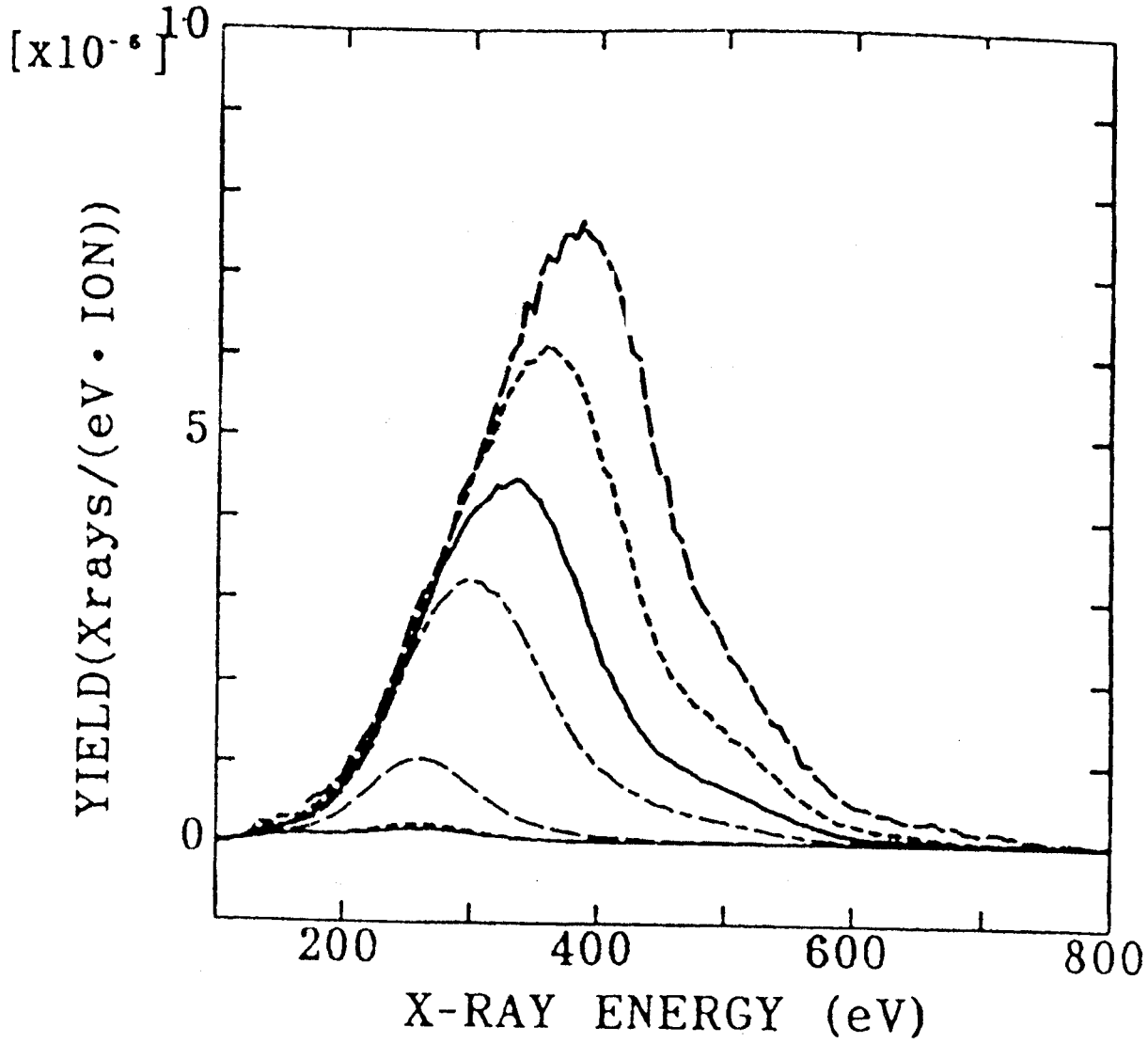

Fig.8(a).

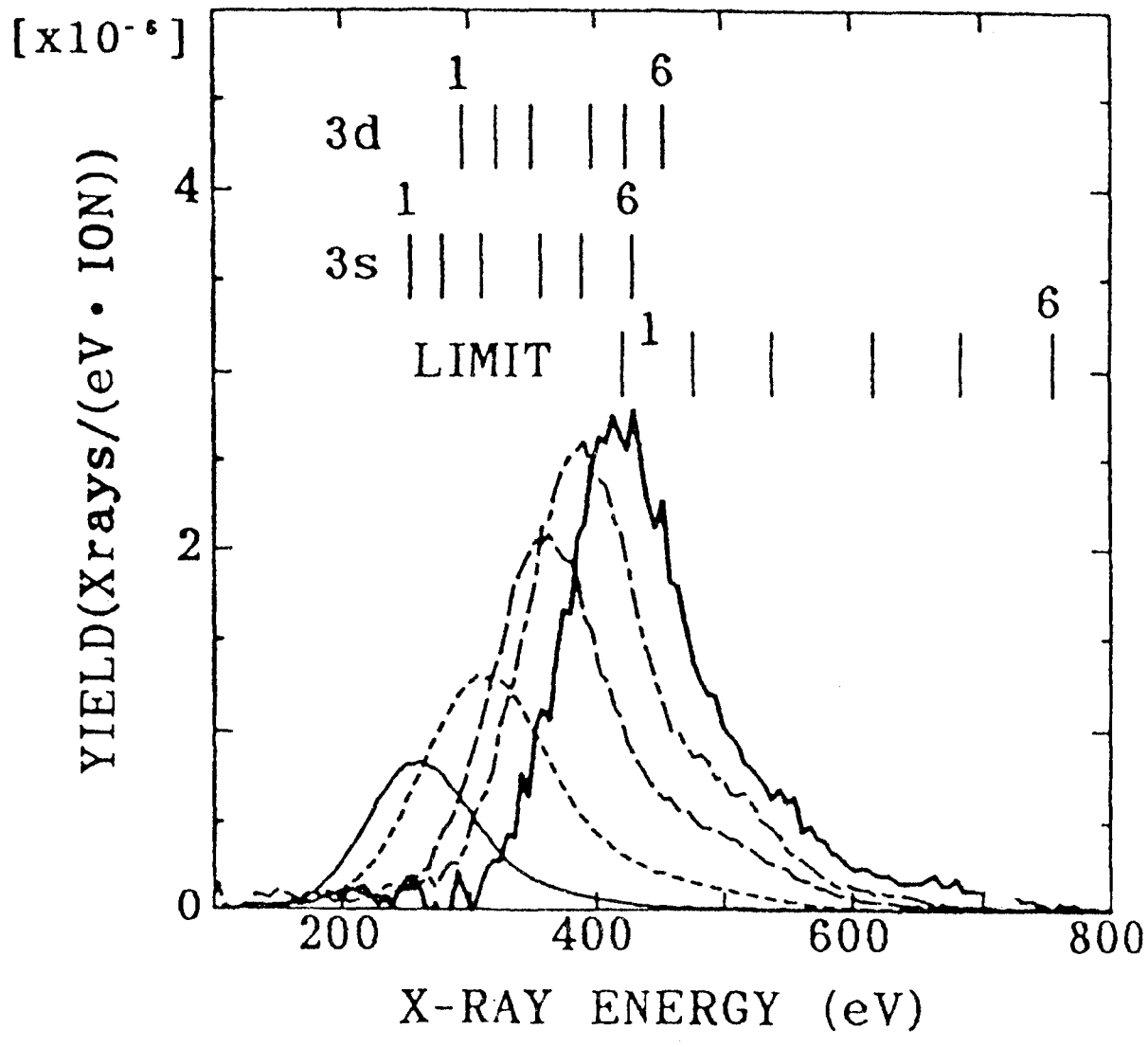
[x10⁻⁶]
YIELD(Xrays/(eV • ION))
1
6
3d
1
6
3s
6
1
LIMIT
4
2
0
200
400
600
800
X-RAY ENERGY (eV)

Fig.8(b).

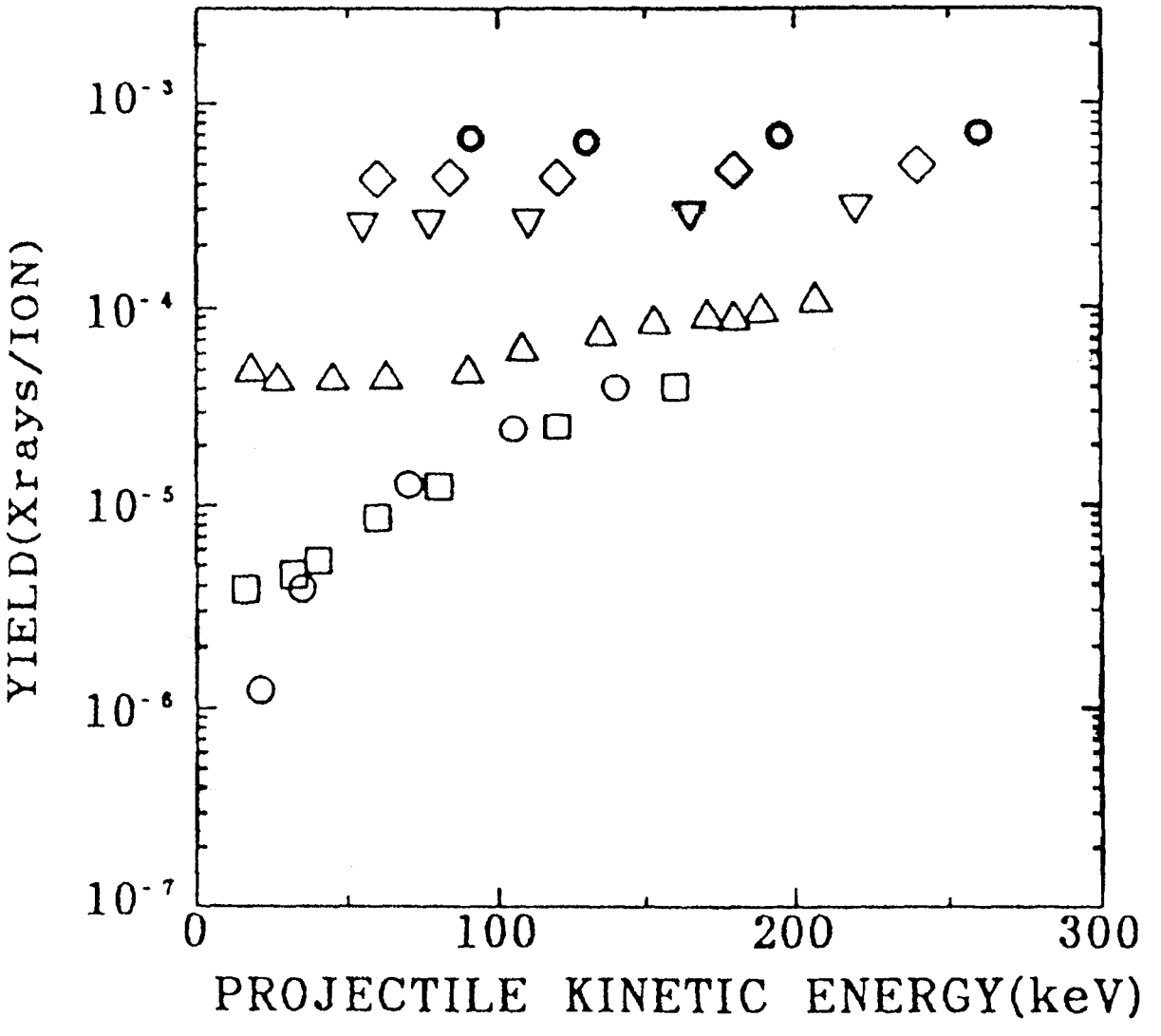
YIELD(Xrays/ION)
10⁻³
10⁻⁴
10⁻⁵
10⁻⁶
10⁻⁷
0
100
200
300
PROJECTILE KINETIC ENERGY(keV)

Fig.9.